Relationships between strain and band structure in Si(001) and Si(110) nanomembranes

C. Euaruksakul,[1] F. Chen,[1,2] B. Tanto,[1] C. S. Ritz,[1] D. M. Paskiewicz,[1] F. J. Himpsel,[1] D. E. Savage,[1] Zheng Liu,[3,4] Yugui Yao,[5] Feng Liu,[3] and M. G. Lagally[1,*]

[1]*University of Wisconsin–Madison, Madison, Wisconsin 53706, USA*

[2]*Xi'an Jiaotong University, Xi'an, Shannxi 710049, China*

[3]*University of Utah, Salt Lake City, Utah 84112, USA*

[4]*Center for Advanced Study, Tsinghua University, Beijing 100084, China*

[5]*Institute of Physics, CAS, Beijing 100190, China*

(Received 9 April 2009; revised manuscript received 19 June 2009; published 24 September 2009)

The flexibility of single-crystal Si nanomembranes allows strain to be applied elastically without introducing dislocations in the fabrication process, resulting in uniform strain. It is also relatively easier to apply different types and orientations of strain to Si using elastic-strain sharing than by the traditional graded-strained-layer approach. We use X-ray absorption spectroscopy to measure the effect of uniform biaxial strain on several features of the conduction band structure of Si with (001) and (110) orientations. By also measuring the Si $2p$ photoelectric threshold, we are able to determine the absolute positions of features of the Si conduction band and their change with strain.

DOI: 10.1103/PhysRevB.80.115323 PACS number(s): 78.40.Fy, 71.70.Fk, 71.20.Mq

I. INTRODUCTION

Applying strain is a practical way to improve the performance of Si devices because the electronic properties of Si are modified by strain. Strain changes the crystal lattice, influencing the band structure in two ways: the volume change shifts positions of energy bands and the lowering of the crystal-symmetry splits degeneracies in bands. With carefully engineered strain, one can (1) shift the conduction band minima to achieve a desired band offset between different materials,[1] (2) create local confinement and periodic band-gap modulation in a single material by creating local strain on the 100 nm scale using epitaxially grown nanostressors,[2] or (3) improve the mobility of the free carriers by eliminating low-mobility channels or reducing scattering via reduction in degeneracy of bands.

In this work, we present detailed measurements of the effects of strain on several features of the conduction band of Si, for two orientations of the Si surface, (001) and (110). We report measurements on Si(110) and elaborate upon our recent work[3] on Si(001), providing detailed descriptions of the experiments and the analysis.

Several efforts to predict the relationship between strain and the band structure of Si have been made. For a summary of these efforts, see Schäffler.[4] The calculations use different methods and yield not always consistent results, presumably due to different starting assumptions or input parameters. Some calculation methods adjust parameters to achieve the measured band-gap energy of strained Si (until recently[3] the only available experimental result). Such adjustments can result in large differences in predictions related to other parts of the conduction band.

Limited experimental data on Si band structure/strain relationships exist for the following reason: in conventional samples, the strain is laterally nonuniform. For a quantitative understanding of the relationship, it is crucial to perform measurements on Si samples that are uniformly strained across the observed area. Conventional strained Si films are grown on a fully relaxed SiGe layer, which has a larger lattice constant than Si.[5] The major drawback of using Si grown on such SiGe substrates for measuring strain/band-structure relationships is that dislocations are introduced during the fabrication of the SiGe layer.[6] These dislocations may lead to dislocation pileups, which cause the lattice constant of the SiGe template to be nonuniform, and therefore also create a laterally nonuniform strain in the Si grown on it. Such a nonuniform strain makes quantification of the effect of strain on band structure unreliable, although the degree to which this is true is currently not known. The changes with strain in energy positions of features in the band structure are in the 10–100 meV range.

Elastically strain sharing nanomembranes[7,8] offer a way to create uniform strain in Si and other materials. The fabrication of such membranes is described in detail elsewhere.[9] Briefly, by growing a three-layer sandwich structure in which the middle layer is strained (but not plastically relaxed, i.e., it is below its kinetic critical thickness) and then releasing the trilayer membrane from its holding substrate, the strain can be shared elastically, without the creation of dislocations. The strain is biaxial in the plane, and via Poisson's ratio, uniaxial normal to the plane. These membranes are used for our measurements of conduction band shifts with strain.

Si nanomembranes (SiNMs), either strained or unstrained, have a wide range of potential applications. This potential has driven recent activity in the development, for example, of high-speed flexible microelectronics,[10] optoelectronics,[11,12] photovoltaics,[13] and other new technologies.[7,14]

We use X-ray absorption spectroscopy (XAS) with electron-yield detection to observe the Si conduction band states as a function of strain. The technique relies on the absorption of synchrotron-generated X rays to create a transition from the Si $2p$ core levels to the conduction band (energy in the range between 99–106 eV, the $L_{II,III}$-to-conduction band transition, $L_{II}=2p_{1/2}$, and $L_{III}=2p_{3/2}$), followed by Auger deexcitation to fill the core holes with valence-band electrons. The ~100 eV Auger electrons scat-

ter inelastically, generating a cascade of secondary electrons. The total electron yield can be obtained by measuring the current to the sample. The probe depth of this total-electron-yield detection is about 5 nm.[15] (The mean escape depth of 100 eV electrons is less than 1 nm, slower electrons will have a somewhat larger escape depth). By scanning the X-ray energy and recording the current at each energy, we measure the joint density of states of the $2p$ levels and the conduction band edge. Because the shape of the $2p$ level is known, a spectrum corresponding to the density of states in the conduction band can, in principle, be created.

For all intents, we determine here only the appearance in transition energy of subbands in the conduction band structure. The fine structure in the XAS spectrum provides this information. An accurate determination requires high energy resolution, in our case 10 meV. Although the details of the density of states in each subband are also inherently contained in the spectra, they cannot be reliably determined.

We performed XAS measurements on Si nanomembranes with a range of biaxial in-plane strain for two different orientations of the surface [(001) and (110)] to measure the effect of strain on the energy position of conduction band features. We analyze the magnitude of degeneracy splitting that occurs in the Δ valley in strained Si(001) NMs and in the L valleys in strained Si(110). We compare our measurements with theoretical predictions of shifting and degeneracy splitting of subbands. We also discuss our approach to determining the absolute shift of conduction band levels (the energy shift relative to the vacuum level) caused by the strain.

II. EXPERIMENT

We made Si(001) NMs with biaxial tensile strain up to 0.950% and Si(110) NMs with biaxial strain up to 0.650%. To fabricate the strained Si(001) membranes, we used chemical-vapor deposition (CVD) in ultrahigh vacuum to create 23 nm Si/107 nm $Si_{0.87}Ge_{0.13}$/28 nm Si and 4 nm Si/69 nm $Si_{0.8}Ge_{0.2}$/9 nm Si structures on Si-on-insulator (SOI) substrates and 13 nm Si/105 nm $Si_{0.7}Ge_{0.3}$/32 nm $Si_{0.8}Ge_{0.2}$ structures on SiGe-on-insulator (SGOI). In each case the middle layer is compressively strained and thus acts as the stressor layer to provide the tensile strain in the top Si layer upon release. The three sandwich structures above create 0.325%, 0.630%, and 0.950% strain on the top Si layer, respectively, after release.[16] For the 0.950% strain sample, SGOI is used as the substrate instead of SOI, so that an elastically strained SiGe stressor film with higher Ge composition and hence higher compressive strain can be grown, allowing in turn a higher tensile strain in the top Si layer. A strained Si(001) layer grown directly on a graded SiGe substrate (no release and no strain sharing) and having a strain of 0.8% was measured as an additional data point. This type of sample is not ideal for strain measurement because it contains dislocations and may contain dislocation pileups and thus nonuniform strain, as we discussed above.

For strained Si(110), we start from SOI with a Si(110) template layer and use molecular-beam epitaxy (MBE) to grow 9 nm Si/81 nm $Si_{0.89}Ge_{0.11}$/10 nm Si, 7 nm Si/ 40 nm $Si_{0.81}Ge_{0.19}$/7 nm Si, and 9.5 nm Si/49 nm $Si_{0.77}Ge_{0.23}$/9.5 nm Si sandwich structures, which produce 0.28%, 0.60%, and 0.65% biaxial tensile strain in the Si(110) layers, respectively, after release. MBE is used because it allows, in contrast to CVD, a decoupling of the growth temperature and the deposition rate, and thus a reasonable rate of growth at lower temperatures. The lower growth temperature helps to limit the nucleation of the stacking faults that are prevalent in the growth of Si(110) (Ref. 17) and also results in much smoother films.[18,19]

Elastically strain sharing NMs automatically suppress dislocation formation but one needs to understand the relaxation mechanisms and design the fabrication process carefully in order to prevent misfit dislocations during the growth and to achieve uniform strain after release. All SiGe stressor layers in every trilayer membrane we grow are metastable before release (which means dislocations can nucleate with enough thermal energy).[20] Thus, for strained Si(001) membranes, we keep the growth temperatures of the SiGe layers in CVD below 600 °C to limit the driving force for the *in situ* strain relaxation by dislocations (i.e., we keep the growth below the kinetic critical thickness for dislocation formation at that temperature). We find that the membranes after release are virtually free of misfit dislocations and are thermally stable at least up to 1100 °C.[21]

In contrast, in the formation of relaxed SiGe substrates via strain grading (conventional process on bulk Si), dislocations *must* be introduced to relax the lattice of SiGe. These dislocations may have several effects: even if there are no misfit dislocations in the final relaxed SiGe layer that serves as the substrate for strained-Si growth, the pileups of these dislocations in lower layers cause nonuniform strain in the final SiGe layer, in addition to crosshatch and certainly threading dislocations through this final layer.[22] The crosshatch is usually polished away and the threading dislocations may not be too important in affecting the subsequent strained Si growth. But any strain nonuniformities are copied into the growing strained-Si layer. Such nonuniformities in strain, in addition to causing local nonuniformities in band positions, will appear in XAS as an average strain.

The intermediate case is the use of SGOI as the substrate, as we did for the 0.950% strained Si sample. The SiGe template layer in SGOI is bonded and smart cut™ from a (plastically) relaxed $Si_{0.80}Ge_{0.20}$ film grown in the conventional manner as the last step in a SiGe graded layer (see above). Misfit dislocations are confined in the layers below the final SiGe layer and thus they are removed by the smart-cut process, leaving only widely separated threading segments, which should not affect our band-structure measurements. Still, any dislocation pileups when the graded layers are made will cause inhomogenities in strain in the final SiGe layer that will be inherited by the template layer of SGOI. All the films grown on SGOI, i.e., the higher-concentration SiGe stressor layer and the ultimate Si layer, may therefore have nonuniform strain prior to the release. However, once the trilayer is released, the strain sharing depends only on the thickness and the composition of each layer, regardless of the initial strain of (or strain distribution in) the unreleased structure. So the structure can relax uniformly over the whole membrane area, resulting in uniformly strained Si in the top layer. We still need to assume that the Ge compositions of

the SiGe template and stressor layers are laterally homogeneous, but this seems not a serious assumption. We can independently confirm, using low-energy electron microscopy, that membranes made on SGOI and released contain no misfit dislocations,[21] in contrast to strained Si fabricated in the conventional way.[6,22] Such results will be presented elsewhere.[21]

Because XAS is so sensitive to the near-surface region and because we are also measuring transitions that involve the work-function (see later) preparation of the surface is important. All samples were placed in ~10% hydrofluoric acid (HF) solution to remove the native-oxide layer before transferring into the XAS vacuum chamber. The transfer process takes less than 10 min. It is known that H termination stabilizes Si surfaces for many hours against reoxidation. We have also independently verified the surface condition after HF treatment as well as the slow reoxidation of SiNMs.[23] The samples were kept for 3–4 h in the vacuum introduction chamber at room temperature before transfer into the ultrahigh-vacuum experimental chamber for the XAS measurement. The surfaces are therefore terminated primarily with H atoms, with possibly small amounts of F, O, and C contamination.

The XAS measurement was performed using synchrotron-generated X rays normally incident on the sample. The electron yield was measured with a picoammeter that was connected to the sample holder via an electrical feed through. To compensate for the change in the beam intensity due to fluctuations of the X-ray intensity during data collection and also for the optical characteristics of the monochromator, we continuously measured the X-ray intensity by monitoring the electron yield from a fine gold mesh placed in front of the sample. By normalizing the XAS total electron yield from the sample with the yield from the gold mesh, we significantly reduced variations in the XAS intensity.

We used linearly polarized X rays from the varied-line-space plane grating monochromator beamline at the University of Wisconsin Synchrotron Radiation Center. The high flux density of X rays generated from undulator magnets allows use of the narrowest monochromator exit slit to select the desired photon energy. This approach minimizes the energy dispersion of the X-ray spot on the sample. With a 10 μm exit slit, we achieved 10 meV energy resolution in our measurements. We bracketed all scans with bulk-Si reference measurements. This procedure allows us to calibrate the energy scale of every spectrum to the L_{III} edge of unstrained Si, known to be at 99.85 eV.[24]

III. RESULTS AND DISCUSSION

A. Strained Si(001)

The measured XAS total-electron-yield spectra for Si(001) membranes with different amounts of strain are compared to an unstrained-Si reference in Fig. 1. The arrows show that the absorption edge of strained Si(001) shifts to higher energy as the tensile strain increases. The absorption edge corresponds to the transition from $2p_{1/2}$ and $2p_{3/2}$ to the Δ valleys of the conduction band. The shapes of the spectra are also affected by strain, something not obvious until we take the derivative of each spectrum, as shown by Fig. 2. Features that appear as shoulders or changes in slope in the absorption edges are accentuated as peaks, each of which is a good representation of a conduction band valley, i.e., the minimum in the energy-momentum relationship where the density of states rises suddenly with increasing energy. The energy positions of the valleys are the values that we can conveniently compare to calculations.

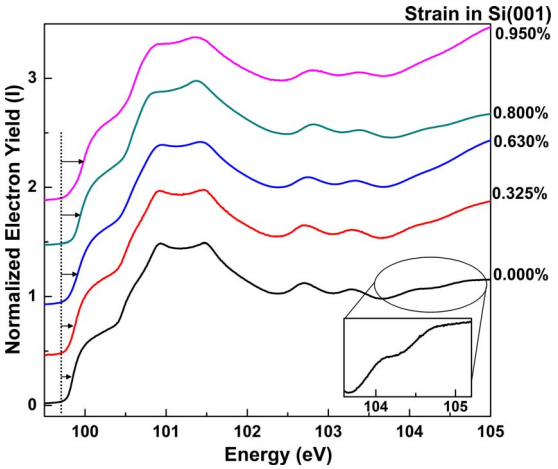

FIG. 1. (Color online) Total-electron-yield XAS spectra from strained Si(001) samples with a bulk Si(001) reference after normalization with the X-ray intensity measured by a gold mesh. Each spectrum is an average of three consecutive measurements. No curve smoothing is performed. The intensity zeros of the curves are offset so that the curves do not overlap. The increasing length of the arrows shows that the absorption edge moves to higher energies with increasing strain. The inset expands the vertical scale for the $2p$ photoelectric threshold of unstrained Si(001).

Because the Si $2p$ core level splits into $2p_{3/2}$ and $2p_{1/2}$ by spin-orbit coupling and the XAS spectra represent the joint density of states between the conduction band and the Si $2p$ levels, the transition from Si $2p$ to each conduction band valley generates two identical peaks, with a separation that remains constant at 0.61 eV (with the assumption that the $2p$ components do not shift by different amounts with strain). Figure 2 shows that the peaks in the derivative spectra shift in different directions with increasing tensile strain. We can analyze the origin of each peak using the existing theoretical prediction from Ref. 25 presented in Fig. 3. The first strong peak, which is obviously created from the optical transition from Si $2p$ to the conduction band minimum Δ, provides a good reference point. As strain increases, the peak shifts toward higher energy and also changes its shape, as can be seen by a small shoulder on the lower-energy side. The biaxial strain along the $\langle 001 \rangle$ orientation splits the sixfold degeneracy of the Δ valleys into twofold degenerate Δ_2 and fourfold degenerate Δ_4 subbands, caused by the difference in the lattice constants in and out of plane. The second pair of peaks, starting at around 101 eV, is from the transition from Si $2p$ to the L_1 valley in the $\langle 111 \rangle$ direction. The peaks shift oppositely, to lower energy, as strain increases and merge with the higher-energy Si $2p$-Δ peak in the highest-strain sample. At about 103 eV, the Si $2p$-L_3 optical transition appears; it shifts to larger energy with tensile strain. These

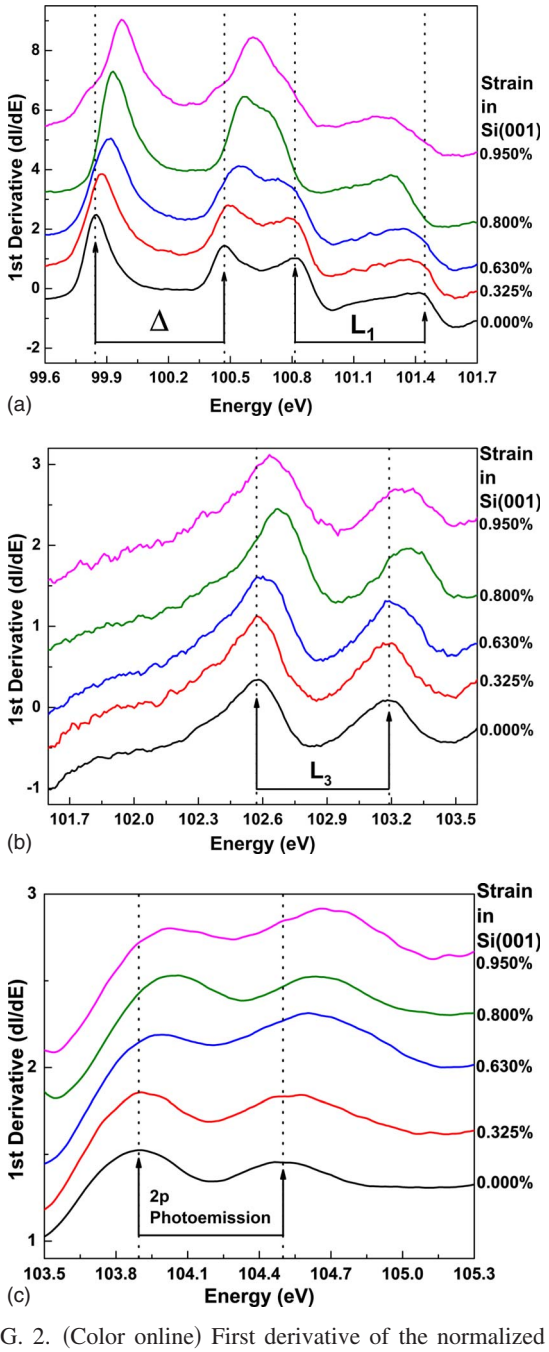

FIG. 2. (Color online) First derivative of the normalized XAS yield, shown in Fig. 1, for unstrained bulk Si(001) and strained Si(001) with biaxial tensile strain up to 0.95%, plotted in different energy ranges: (a) between 99.6–101.7 eV showing peaks from Si $2p$-Δ and Si $2p$-L_1 transitions, (b) between 101.6–103.6 eV showing peaks from the Si $2p$-L_3 transition, and (c) between 103.5–105.3 eV showing peaks representing the Si $2p$ photoelectric thresholds. The peak arising from each transition is duplicated because of the spin-orbit splitting of the Si $2p$ core level (by 0.61 eV), with the transitions from the $2p_{3/2}$ level at lower energy for each line. All plots are smoothed by nine-point Savitzky-Golay smoothing after differentiation. The plot in (c) is further smoothed with 21-point adjacent averaging to suppress the noise. All curves are offset in y for ease of viewing. The vertical scale in each panel is enhanced by a factor proportional to the peak strength in each energy range to emphasize the peak positions; hence peak magnitudes cannot be compared across panels.

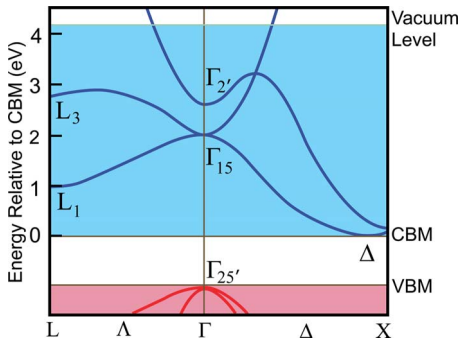

FIG. 3. (Color online) The predicted band structure of Si, calculated by Chelikowsky and Cohen (Ref. 25). Several valleys are shown at different high-symmetry points. We use the prediction as a map to identify the peaks in the XAS spectra.

higher-lying L_1 and L_3 conduction band valleys are obviously not accessible by electronic-transport measurements.

The predictions of Ref. 25 suggest that there are two direct-bandgap valleys at the Γ point with energies 2 and 3 eV above the Δ valley (Γ_{15} and $\Gamma_{2'}$) but they are barely observed in the spectra because the dipole selection rules[26] prohibit the transition from the Si $2p$ level to these valleys. These transitions thus are not included in our data analysis. At 104 eV, we can observe two more peaks that shift toward larger energy. Despite appearing in the same measurement, they are created via a different mechanism. This emission of electrons appears when the X-ray energy is greater than the photoelectric threshold of the Si $2p$ core level (the distance from the core level to the vacuum level). The appearance energy is consistent with the reported electron affinity of Si (χ=4.1 eV).[27]

To find the magnitude of the degeneracy splitting of the Δ valley by strain, we fitted the peak shape of strained Si by a spectrum created from the peak shape of the unstrained Si (for which the Δ subbands are degenerate) with proper intensity ratio representing each subband, in this case 1:2 for Δ_2:Δ_4. We therefore scale the Δ peak shape of unstrained Si with 1/3 and 2/3 factors to create Δ_2 and Δ_4 representations, as shown by Fig. 4. We use these to fit the strained-Si spectra, with the splitting value, $\Delta E_{\Delta}^{split}$, and the center of gravity shift as variables, to find the shift and the amount of the splitting for each magnitude of strain. We can measure the shifts of the L valleys directly from the peak positions, because the symmetry of the L point is not changed by a biaxial strain in the (001) plane, so there is no splitting of the L_1 and L_3 valleys. All of these optical transitions to the conduction band valleys are plotted in Fig. 5(a). It must be remembered that these shifts of the optical-transition energy do not represent the direction in energy nor magnitude of the absolute shifts (which are relative to the vacuum level), because the XAS measurement uses the Si $2p$ core level as reference, which is also shifted by strain.[28] Still, these optical-transition data provide useful information about the changing relative positions among the conduction band valleys and the relative shifts caused by strain. The directions of the relative shifts between the valleys and the splitting are in good agreement with theoretical calculations.[2,29–33] Fig. 5(a) shows, for example, that the L_1 valley shifts down toward the Δ valley,

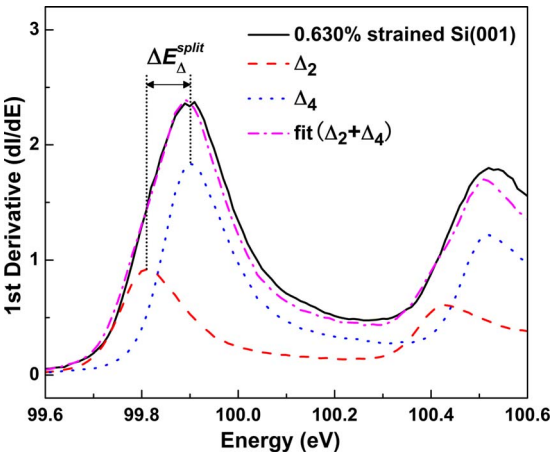

FIG. 4. (Color online) Curve fitting to find the amount of Δ valley splitting in Si(001). The fitting of data for 0.630% strained Si(001) is given as an example. The solid line shows the first-derivative spectrum of the measurement, for the transitions from both the $2p_{3/2}$ and $2p_{1/2}$ levels. Two fitting curves are created from the peak shape of unstrained Si, with 1/3 and 2/3 multiplicity ratios representing Δ_2 (dashed) and Δ_4 (dotted), respectively. The splitting magnitude, $\Delta E_{\Delta}^{split}$, and the shift are parameters to create a fit (dash-dotted) that matches the strained-Si curve.

reducing the gap between them at a rate greater than linear, which is consistent with predictions.[32,33] The L valley is in the ⟨111⟩ direction with atoms therefore closer to each other than those in the directions of the Δ valleys, ⟨100⟩.

We can also measure the Si $2p$ photoelectric threshold with XAS. The threshold gives (with certain assumptions) the absolute position the Si $2p$ levels in strained Si. Hence we can correct the shifts in the optical-transition energies in Fig. 5(a) to obtain the absolute shift of each conduction band valley. The photoelectric onsets near 104 eV in Fig. 1 become peaks after taking a first-order derivative, as seen in Fig. 2(c). The shift of these peaks with strain is emphasized by replotting the derivative spectra between 103.6–104.8 eV with a gray scale, as shown by Fig. 6. We need to assume only that the work function is stable during all measurements (i.e., the surface contamination rate is minimal, a good assumption with H-terminated surfaces in vacuum).

To extract quantitative information, we analyze peak positions carefully. Figure 2(c) shows that the background differs for the several spectra but not in a consistent manner with changing strain. These differences are likely due to differences in the magnitude of the oxide peak at 107 eV, which is sensitive to even very small amounts of oxygen on the surface. To analyze the position of the Si $2p$ level accurately, we take the second derivative of the electron-yield spectra. We then fit the second-derivative peaks with derivatives of two Gaussian peaks to find the position of the Si $2p$ levels in each strained sample, with the results plotted in Fig. 5(b). Figure 7 shows the absolute shift of the Δ, L_1, and L_3 conduction band valleys created by combining the optical-transition shift in Fig. 5(a) and the $2p$ core-level shift in Fig. 5(b). This complete analysis then shows that all three conduction band valleys shift downward with tensile strain but

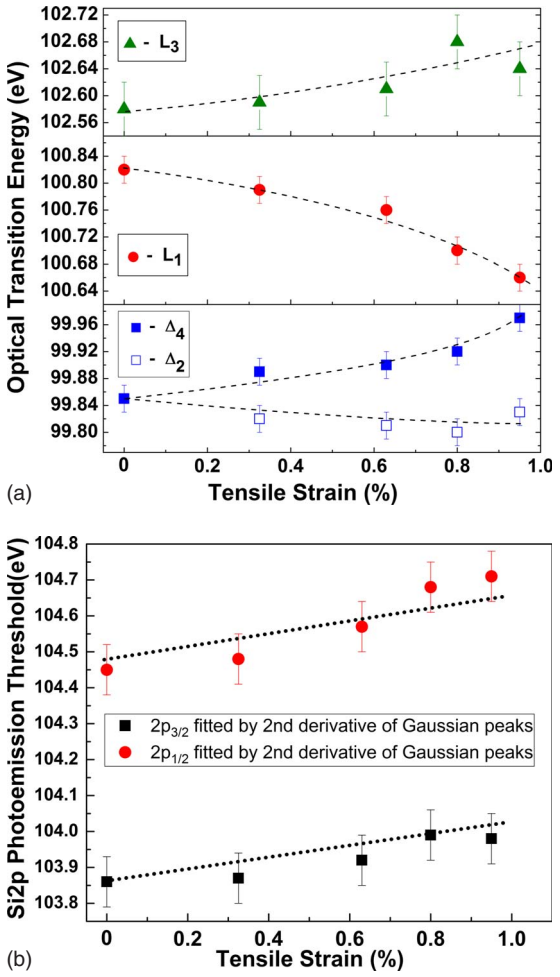

FIG. 5. (Color online) (a) Summary of the XAS measurements on Si(001). (a) Optical-transition energies from $2p$ to Δ, L_1, and L_3 conduction band valleys versus strain. The Δ valley splits at a constant rate. The $2p$-L_1 transition energy decreases at a greater than linear rate, reducing the gap between Δ and L_1. (b) The photoelectric threshold for Si(001) at different strains. The increase in the energy means that the core electrons become more tightly bound as strain increases.

at different rates. The Δ and L_3 valleys shift down (to larger energies relative to the vacuum level) almost linearly and the L_1 valley shifts with higher slope that increases with tensile strain.

B. Strained Si(110)

A part of the strain-conduction band relationship that has not previously been measured is the splitting of the L valley in Si with strain. Our prior measurements[3] on Si(001) cannot determine it, because, as we pointed out, biaxial strain on the (001) plane, does not split the L valley. In contrast, when biaxial strain is applied to Si(110) not only the Δ-valley but also the L-valley degeneracy is split. Figure 8 shows the splittings of these two valleys schematically. We have measured the splitting of the L valley in Si(110) nanomembranes tensilely strained from 0.28% to 0.65% with XAS and compared them to a bulk unstrained Si(001) reference. The first

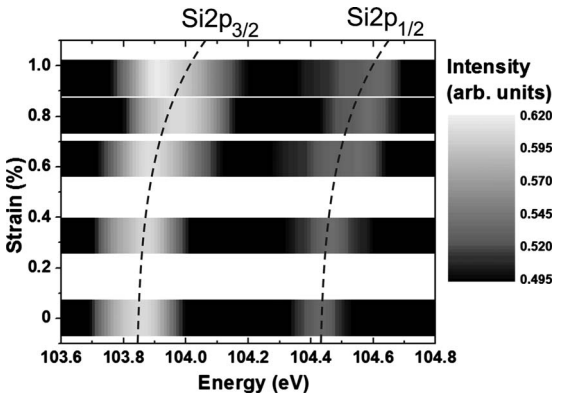

FIG. 6. A contour plot of the derivative spectrum in Fig. 2(c) in the energy range of the Si 2*p* photoelectric threshold (103.6–104.8 eV) with the derivative magnitude shown by gray scale bar. The shift of the Si 2*p* core level with strain is evident.

derivatives of their electron-yield spectra are shown in Fig. 9. The energy shift of the features and a broadening of the Si $2p$-L_1 optical-transition peak from the degeneracy splitting are evident. To find the splittings of the valleys in the Si(110) membrane, we fit the data in the same manner as we did to measure the degeneracy splitting of the Δ valley in strained Si(001). Biaxial strain in the (110) plane splits (see Fig. 8) the sixfold Δ valley into twofold and fourfold degenerate subbands, and the eightfold L_1 valley into two fourfold degenerate subbands. From the number of valleys in each subband, the fitting for Δ can be made using a 1:2 intensity ratio used in strained Si(001), and a 1:1 ratio for L_1 to create subband representations. The fits for Δ and L_1 for 0.60% strained Si(110) are shown by Figs. 10(a) and 10(b), respectively. We summarize the shifts versus strain in the optical-transition energy and the magnitudes of the splitting from the fits to the Δ and L_1 spectra in Si(110) in Fig. 11.

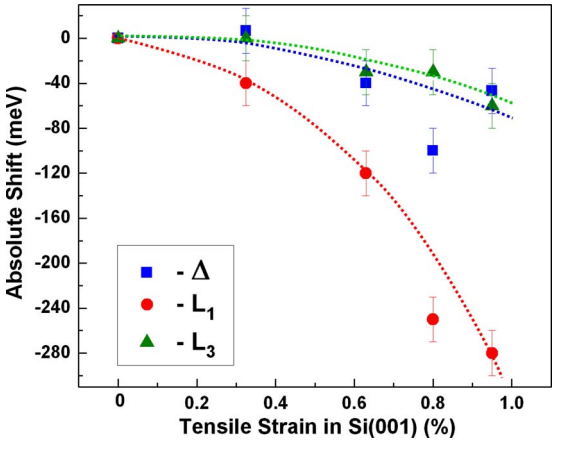

FIG. 7. (Color online) The absolute shift of Δ (center of gravity), L_1, and L_3 conduction band valleys of Si(001) with tensile strain. All conduction band valleys shift down with strain, consistent with the most recent calculation (Ref. 36). The rapid and nonlinear energy shift for L_1 is evident. The lines are aids to the eye and not fits.

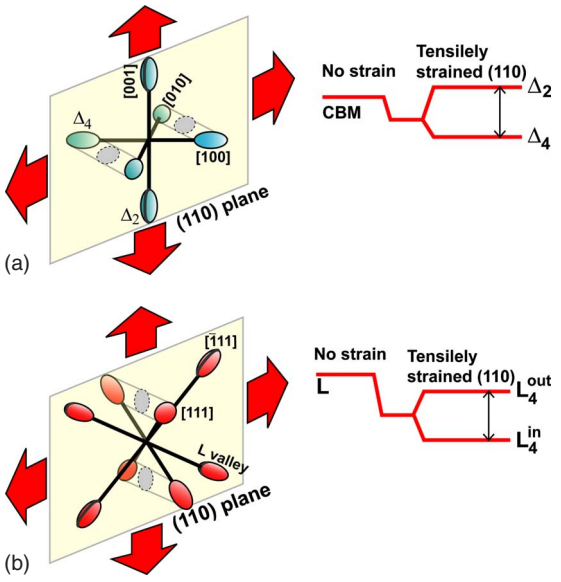

FIG. 8. (Color online) Degeneracy splitting of conduction band valleys due to biaxial tensile strain in Si(110) NMs. (a) Δ splits into twofold and fourfold degenerate subbands. (b) L splits into two fourfold degenerate subbands.

C. Comparisons to theoretical predictions

We can compare these results with the existing theoretical prediction, using linear deformation-potential theory, by Herring and Vogt.[34] The shift of an individual conduction band valley (distinguished by its direction in momentum space among the degenerate valleys) follows the equation

$$\Delta E^{ijk} = [\Xi_d \overleftrightarrow{1} + \Xi_u(\hat{a}_{ijk} \otimes \hat{a}_{ijk})]:\overleftrightarrow{\varepsilon}, \quad (1)$$

where ΔE^{ijk} is the energy shift of an individual conduction band valley sitting in the $\langle ijk \rangle$ direction, $\hat{a}_{ijk}$ is a unit vector along the direction of the valley ijk, $\overleftrightarrow{1}$ is a unit tensor, and $\overleftrightarrow{\varepsilon}$ is the strain tensor. $\hat{a}_{ijk} \otimes \hat{a}_{ijk}$ denotes a self-dyadic product of $\hat{a}_{ijk}$. For strained Si(001), the in-plane strain $\varepsilon_{\parallel}$ is equal to ε_{xx}

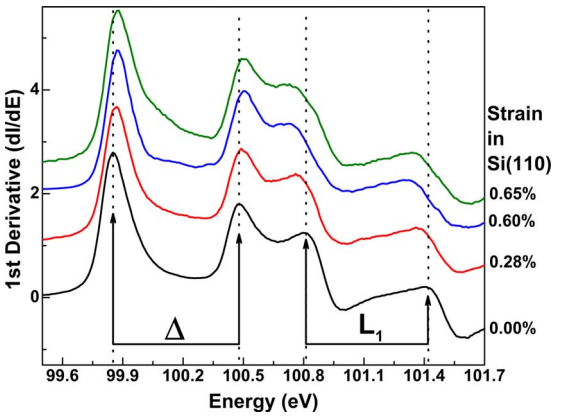

FIG. 9. (Color online) Comparison of the XAS derivative spectra of Si(110) membranes for strain from 0.28% to 0.65% and an unstrained-bulk-Si(001) reference. The transitions from $2p_{3/2}$ and $2p_{1/2}$ levels are indicated.

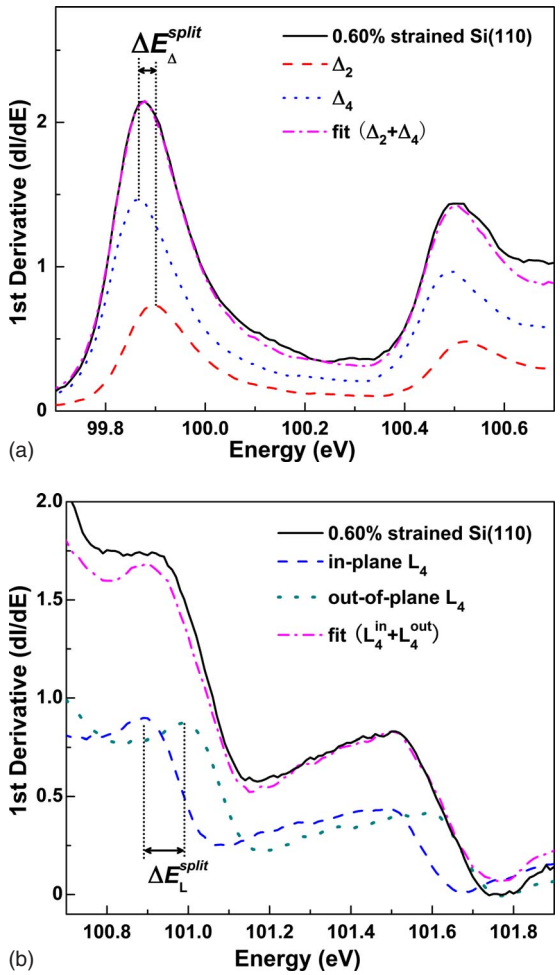

FIG. 10. (Color online) Data fitting procedure to find strain-induced splitting in Si(110). (a) Between Δ_2 and Δ_4 in a strained Si(110) NM. Δ_2 moves to higher energy than Δ_4; the direction is opposite of that for strained Si(001). (b) For the L_1 valley. The strain splits L_1 into two fourfold degenerate subbands. $\Delta E_{\Delta}^{split}$ and ΔE_{L}^{split} show the split in each case.

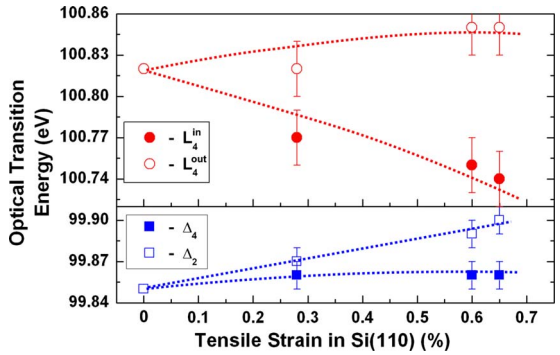

FIG. 11. (Color online) Summary of the XAS measurements on Si(110), showing the optical-transition energies from $2p$ to Δ and L_1 conduction band valleys versus strain. Both Δ and L_1 valleys split with strain. The gap between Δ and L_1 average values decreases in the same manner as in tensilely strained Si(001). The dashed lines show the trends of the subband shifts.

and ε_{yy}, and the out-of-plane strain $\varepsilon_{\perp}$ is ε_{zz}, with all shear strain components equal to zero. This makes the strain tensor

$$\overleftrightarrow{\varepsilon} = \begin{bmatrix} \varepsilon_{xx} & \varepsilon_{xy} & \varepsilon_{xz} \\ \varepsilon_{yx} & \varepsilon_{yy} & \varepsilon_{yz} \\ \varepsilon_{zx} & \varepsilon_{zy} & \varepsilon_{zz} \end{bmatrix} = \begin{bmatrix} \varepsilon_{\parallel} & 0 & 0 \\ 0 & \varepsilon_{\parallel} & 0 \\ 0 & 0 & \varepsilon_{\perp} \end{bmatrix}. \quad (2)$$

Following solid-mechanics theory,[4] $\varepsilon_{\perp} = -D^{i}_{(001)}\varepsilon_{\parallel} = -2(\frac{c_{12}}{c_{11}}) \times \varepsilon_{\parallel} = -0.78\varepsilon_{\parallel}$ for Si. The strain value ε is positive for tensile strain and negative for compressive strain. Using the strain tensor in Eq. (2), we find the splitting between out-of-plane Δ_2 and in-plane Δ_4

$$\Delta E_{\Delta}^{split} = \Delta E_{\Delta}^{100} - \Delta E_{\Delta}^{001} = \Xi_u^{\Delta}(\varepsilon_{\perp} - \varepsilon_{\parallel}) = 1.78\Xi_u^{\Delta}\varepsilon_{\parallel}. \quad (3)$$

ΔE_{Δ}^{av} is the center of mass of Δ, defined by the average of the energy of the valleys weighted by the number of the valleys in each subband.

$$\Delta E_{\Delta}^{av} = \Delta E_{\Delta}^{001} + \frac{2}{3}(\Delta E_{\Delta}^{100} - \Delta E_{\Delta}^{001}) = \left(\Xi_d^{\Delta} + \frac{1}{3}\Xi_u^{\Delta}\right)(2\varepsilon_{\parallel} + \varepsilon_{\perp}). \quad (4)$$

The term $(\Xi_d + \frac{1}{3}\Xi_u)$ is defined as the deformation potential for the absolute shift of the average energy levels of the Δ valleys (sometimes presented as a_c). For a hydrostatic strain, where $\varepsilon_{xx} = \varepsilon_{yy} = \varepsilon_{zz}$, the energy shifts of all valleys are equal to Eq. (4), thus the term $(\Xi_d + \frac{1}{3}\Xi_u)$ is sometimes called a "hydrostatic deformation potential." Despite the name, the average shift ΔE_{Δ}^{av} does not necessarily represent the shift due to a hydrostatic strain and, to prevent confusion, is not called a hydrostatic shift here. The term $(2\varepsilon_{\parallel} + \varepsilon_{\perp})$ is equal to the volume change $(\Delta V/V_0)$ in the material after applying strain.

To find the splitting of Δ in strained Si(110), we again use Eq. (1) with strain tensor

$$\overleftrightarrow{\varepsilon}_{110} = \begin{bmatrix} \frac{1}{2}(\varepsilon_{\parallel} + \varepsilon_{\perp}) & \frac{1}{2}(\varepsilon_{\parallel} - \varepsilon_{\perp}) & 0 \\ \frac{1}{2}(\varepsilon_{\parallel} - \varepsilon_{\perp}) & \frac{1}{2}(\varepsilon_{\parallel} + \varepsilon_{\perp}) & 0 \\ 0 & 0 & \varepsilon_{\parallel} \end{bmatrix}, \quad (5)$$

(see the proof in Ref. 35) with $\varepsilon_{\perp} = \frac{(c_{11}+3c_{12}-2c_{44})}{(c_{11}+c_{12}+2c_{44})}\varepsilon_{\parallel} = -0.51\varepsilon_{\parallel}$. Two of the sixfold degenerate Δ valleys lie in the (110) plane while the rest have components both in and out of plane [Fig. 8(a)]. Using Eq. (1) with the strain tensor $\overleftrightarrow{\varepsilon}_{110}$ from Eq. (5), we find the splitting of Δ in strained Si(110)

$$\Delta E_{\Delta,(110)}^{split} = \Delta E_{\Delta}^{001} - \Delta E_{\Delta}^{100} = \frac{1}{2}\Xi_u^{\Delta}(\varepsilon_{\parallel} - \varepsilon_{\perp}) = 0.75\Xi_u^{\Delta}\varepsilon_{\parallel}. \quad (6)$$

Of the eight degenerate L valleys, four of them lie in the (110) plane and the rest have both in-plane and out-of-plane components [Fig. 8(b)]. The splitting of L is

TABLE I. A summary of deformation potentials from theoretical predictions and from our XAS measurements on strained SiNMs with (001) and (110) surface orientations. The shift deformation potential of L_1 is not constant but increases with tensile strain. All values are in eV.

Deformation potential	Theoretical prediction	XAS measurement
Δ shift $(\Xi_d^{\Delta}+\frac{1}{3}\Xi_u^{\Delta})$	1.49[a], 4.18[b], −10.06 [c]	−4.02
Δ splitting (Ξ_u^{Δ})	9.16[a], 9.16[d], 9.0[e], 8.79[e], 9.01[e]	8.3 (001), 6.6 (110)
L_1 shift $(\Xi_d^{L1}+\frac{1}{3}\Xi_u^{L1})$	−0.66 [b]	From −10.1 to −40.9
L_1 splitting (Ξ_u^{L1})	16.14[d], 15.9[e], 13.85[e], 15.1[e]	16.5

[a]Our calculation.
[b]Van de Walle (Ref. 37).
[c]Li *et al.* (Ref. 36).
[d]Van de Walle and Martin (Ref. 29).
[e]Rideau *et al.* (Ref. 32).

$$\Delta E_{L,(110)}^{split} = \Delta E_L^{111} - \Delta E_L^{\bar{1}11} = \frac{2}{3}\Xi_u^L(\varepsilon_{\parallel} - \varepsilon_{\perp}) = 1.01\Xi_u^L\varepsilon_{\parallel}. \tag{7}$$

So from the measurement of the L valley splitting in Si(110) nanomembranes, the value of Ξ_u^L can be calculated. Deformation potentials determined from our measured shifts and splittings of the Δ and L_1 valleys in strained SiNMs are listed in Table I and compared to theoretical predictions by Refs. 29, 32, 36, and 37. The splitting deformation potentials of both Δ and L_1 from the measurements are in good agreement with the theory. The measured shift and splitting deformation potentials of L_1 are also reported.

Care must be taken to compare the absolute-shift deformation potential $(\Xi_d+\frac{1}{3}\Xi_u)$ derived from our measurement and from theoretical predictions. Here, in contrast to the splitting, the amount of the energy shift depends on how the reference level is used. The absolute shift by definition uses the vacuum level as a reference. In semiconductors, charge on or near the surface can lead to a surface potential and band bending, a rigid shift of all energy levels that is highest at the surface and falls off into the bulk depending on the doping (Debye length). This surface potential adds to or subtracts from the bulk work function, i.e., the vacuum-level shifts relative to the Fermi level. The band bending causes the threshold for the emission of a Si $2p$ electron created deep in the bulk of the material (outside the region of band bending) to be lower by the surface potential[38] as shown in Fig. 12. The degree of band bending is affected by the surface condition and may also be affected by strain.

Because all the energy levels shift rigidly if a surface potential exists, emission for the strict surface region reflects the situation from the bulk if there were no band bending. In other words, one measures the proper energy difference between the $2p$ and vacuum levels. Fortunately, the probe depth for the appearance of photoelectrons in Si is shallow (mean-free path ~10 nm). In addition, the membranes used here are nominally undoped, which implies that the field from any surface charge changes very slowly and thus the band bending reaches far into the material. Hence any uncertainty in the threshold energy of the $2p$ levels should be negligible in our SiNMs. Therefore the interpretation of the appearance of photoemission from the $2p$ levels should be a good indicator of the energy difference between the $2p$ levels and the vacuum level. It should further be reemphasized that the XAS measurements are sensitive to nearly the same sample volume, allowing the use of the photoelectron appearance energies to be used to produce absolute-energy scales.

Any electric field from surface dipoles[39] created by impurities left on the surface by the HF treatment can also change the electron affinity and thus the electron emission threshold but this influence from the dipoles is unlikely to be affected by strain. We treated all membranes with HF and then loaded them into the vacuum chamber within almost the same amount of time so the effect must be similar for all samples and should change very slowly over time in the vacuum system.

We find the deformation potential of Δ is negative (the valley shifts down with tensile strain) in agreement with the

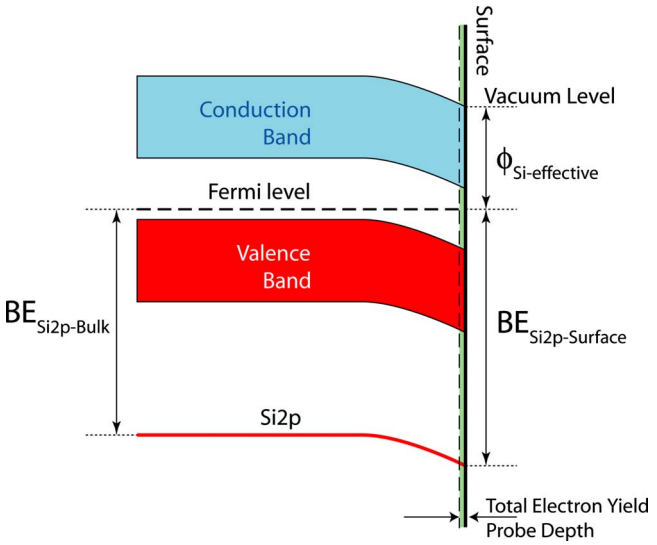

FIG. 12. (Color online) Band bending due to the surface. A p-doped semiconductor is illustrated. The binding energy, relative to the Fermi level, is smaller deep inside the material. The space-charge region reaches into the bulk for long distances for low doping, implying that the potential changes little in the region being probed.

latest calculations[36,40] but opposite to results in earlier ones.[33,41] The direction of the L_1 [both (001) and (110)] absolute shift is consistent with all predictions. As mentioned, we find that the shift of the L_1 valley is nonlinear; thus the deformation potential is not constant but instead increases with tensile strain.

We also perform a calculation to determine the transition energy from the core level to different conduction band valleys for both strain directions and for both orientations to make a more direct comparison with experiments. The calculations are done using the first-principles density-functional theory method with a linear-combination-of-atomic-orbitals basis as implemented in the SIESTA code.[42] Strain is applied relative to the theoretical equilibrium lattice constant of 5.417 Å obtained from total-energy minimization. In concert with the experimental conditions, the biaxial strain applied to the (001) membrane is modeled by the two-atom primitive cell with its cell dimensions fixed equally in the [100] and [010] directions to the desired amount of strain and fully relaxed in the [001] direction. The biaxial strain applied to the (110) membrane is modeled by a four-atom tetragonal unit cell with its cell dimensions strained equally in the $[1\bar{1}0]$ and [001] directions and relaxed in the [110] direction. Our calculation shows that $\varepsilon_{\perp}^{001}=-0.84\varepsilon_{\parallel}^{001}$ and $\varepsilon_{\perp}^{110}=-0.52\varepsilon_{\parallel}^{110}$, which agrees well with the solid-mechanics theory.

As has long been known, the difficulty in deformation-potential calculations lies in the requirement to establish an absolute energy scale, which, however, is usually missed in bulk calculations because of the ill-defined average electrostatic potential.[43] The standard solution is to construct a "supercell" containing both strained and unstrained regions.[44] However, in the supercell geometry, strain can only be applied in one direction, which prevents direct comparison with experimental conditions. In SIESTA'S methodology, the average electrostatic potential is added back to the Hamiltonian as a superposition of atom potentials,[45] which in spirit is very similar to Van de Walle's model-solid approach.[37] As a result, the drifting of zero energy level under strain can be largely eliminated, which enables us to obtain the band shifting under all kinds of strain from separate bulk calculations. We have conducted tests by comparing our results with supercell calculations, when strain is only applied along one direction. It is found that the separate bulk calculation using SIESTA can reproduce well the band shifting, with error smaller than 10 meV.

In the calculations, only valence electrons are treated while core electrons are replaced by pseudopotentials, i.e., only the response of valence levels (valence band or conduction band levels) to strain is calculated while the core levels are effectively frozen. If we compare the calculated shifts of valence levels as a function of strain to the measured transition energies from $2p$ core levels to different conduction band minima, as shown in Fig. 13 for both (001) and (110) nanomembranes, we can determine to what degree the frozen-$2p$-level assumption matches the experiment. Overall the calculated directions and magnitudes of shifts, as well as the relative positions of different valleys, agree well with the XAS data, especially for (110) membranes.

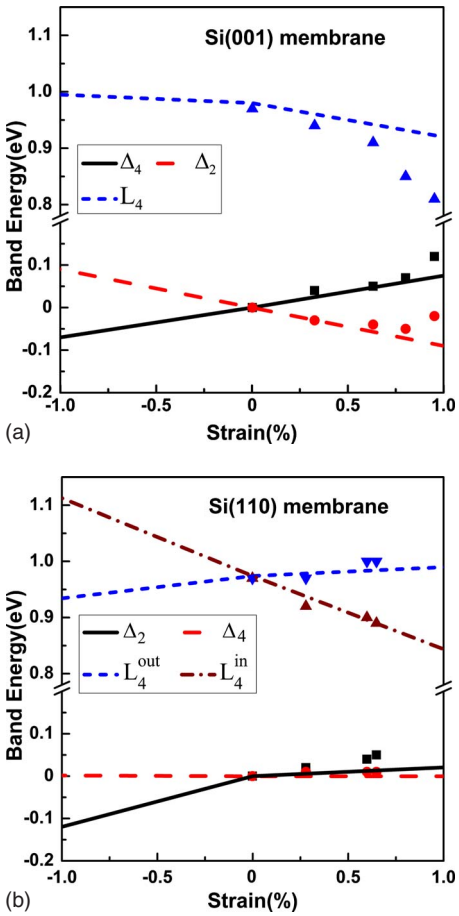

FIG. 13. (Color online) Calculated strain dependence of the energies of different conduction band valleys assuming a frozen $2p$ core level (lines), compared to experiments (dots). (a) (001) membrane and (b) (110) membrane. Positive values are tensile strain. Band energies are measured from the conduction band minimum at zero strain.

One interesting point to note is that the $2p$-to-Δ_4 transition energy in the (110) membrane [Fig. 13(b)] is almost independent of strain, as seen in both experiment and theory. This effect is caused by the cancellation of the biaxial strain in the (110) plane ($\varepsilon_{\parallel}$) and uniaxial strain along the $\langle 110\rangle$ direction ($\varepsilon_{\perp}$, which is of the opposite sign according to the Poisson ratio). From our calculation, we extracted the deformation-potential parameters of silicon as $\Xi_u=9.16$ eV and $\Xi_d+\frac{1}{3}\Xi_u=1.49$ eV. Applying these parameters, we can calculate the strain-induced shift of the Δ_4 energy in the (110) membrane as the formula

$$E(\Delta_4)=\Xi_d(2\varepsilon_{\parallel}+\varepsilon_{\perp})+\Xi_u\frac{1}{2}(\varepsilon_{\parallel}+\varepsilon_{\perp})=0.07\varepsilon_{\parallel}, \quad (8)$$

which shows a very weak strain dependence, consistent with the observation. In contrast, we find the strain dependence of the Δ_4 energy shift in the (100) membrane is about two orders of magnitude greater.

The greater rate of change with strain of the energy of the L_1 valley compared to that of the Δ valley is a result of both the XAS measurements and of our calculation. The result

seems counter intuitive because the position of the L point in the Brillouin zone suggests less sensitivity to biaxial strain on the (001) plane than the *X* point. The L valley is in the ⟨111⟩ directions and thus atoms are closer to each other than those for the Δ valleys, in the ⟨100⟩ directions. But strain in this system will also affect the bending of bonds, not just stretching. In fact, for biaxial strain in the (001) oriented membrane, nearest-neighbor bonds, which are in the ⟨111⟩ directions, are primarily bent.[46] It is possible that the position of the L_1 valley with strain is related to the bending of bonds. Clearly the dependence of shifting and splitting of different components of the conduction band structure on strain is not simple.

D. Conclusions

We have quantitatively measured the influence of strain on features of the conduction band structure of Si with (001) and (110) orientations, using elastically strain sharing Si nanomembranes and XAS with 10 meV energy resolution. The shifts not only of the minimum of the conduction band but also of other critical points at higher energies not accessible by electronic-transport measurements are quantified. We present measurements on the Si(110) orientation, including L-valley splitting, and elaborate on our recent work on Si(001) nanomembranes.[3] We show in detail how to extract absolute energy shifts and how strain affects these shifts. We perform calculations of this shift with strain, assuming frozen $2p$ levels. The comparison with experiment is excellent. We believe this type of information can be a useful input for more accurate all-electron calculations of strained Si. Elastically strain sharing nanomembrane technology enables considerably higher strain as well as strain in other materials and one can thus expect a continued emphasis on evaluating how strain influences band structure. Of particular interest in these future experiments will be the relative shifts of different conduction band valleys and especially the isolation of particular levels via increased splitting, as well as the cooperation or competition of strain and quantum size effects in very thin membranes.

ACKNOWLEDGMENTS

This work was supported primarily by the U.S. Department of Energy, Office of Basic Energy Sciences, under Grant Nos. DE-FG02-03ER46028 and DE-FG02-03ER46027. Added support came from the Air Force Office of Scientific Research, under Grant No. FA9950-06-1-0472 and from NSF/MRSEC under Grant No. DMR-0520527. The UW-Madison Synchrotron Radiation Center is supported by NSF under Grant No. DMR-0537588. The 0.8% strained Si was provided by Bin Yang, IBM Research Center, Yorktown Heights, NY 10598. C.E. was supported by the Thai government. D.P. was supported by NDSEG. F.C. was supported by the Chinese Scholarship Council. Y.Y. is supported by NSFC (Grant No. 10674163).

*lagally@engr.wisc.edu

[1] G. Abstreiter, H. Brugger, T. Wolf, H. Jorke, and H. J. Herzog, Phys. Rev. Lett. **54**, 2441 (1985).
[2] D. Yu, Y. Zhang, and F. Liu, Phys. Rev. B **78**, 245204 (2008).
[3] C. Euaruksakul, Z. W. Li, F. Zheng, F. J. Himpsel, C. S. Ritz, B. Tanto, D. E. Savage, X. S. Liu, and M. G. Lagally, Phys. Rev. Lett. **101**, 147403 (2008).
[4] F. Schäffler, Semicond. Sci. Technol. **12**, 1515 (1997).
[5] J. W. P. Hsu, E. A. Fitzgerald, Y. H. Xie, P. J. Silverman, and M. J. Cardillo, Appl. Phys. Lett. **61**, 1293 (1992).
[6] P. M. Mooney and J. O. Chu, Annu. Rev. Mater. Sci. **30**, 335 (2000).
[7] S. A. Scott and M. G. Lagally, J. Phys. D **40**, R75 (2007).
[8] M. G. Lagally, MRS Bull. **32**, 57 (2007).
[9] M. M. Roberts, L. J. Klein, D. E. Savage, K. A. Slinker, M. Friesen, G. K. Celler, M. A. Eriksson, and M. G. Lagally, Nature Mater. **5**, 388 (2006).
[10] H.-C. Yuan, Z. Q. Ma, M. M. Roberts, D. E. Savage, and M. G. Lagally, J. Appl. Phys. **100**, 013708 (2006).
[11] H.-C. Yuan, J. Shin, G. X. Qin, L. Sun, P. Bhattacharya, M. G. Lagally, G. K. Celler, and Z. Q. Ma, Appl. Phys. Lett. **94**, 013102 (2009).
[12] L. Chen, Z. X. Qiang, H. J. Yang, H. Q. Pang, Z. Q. Ma, and W. Zhou, Opt. Express **17**, 8396 (2009).
[13] J. Yoon, A. J. Baca, S.-I. Park, P. Elvikis, J. B. Geddes III, L. F. Li, R. H. Kim, J. L. Xiao, S. D. Wang, T.-H. Kim, M. J. Motala, B. Y. Ahn, E. B. Duoss, J. A. Lewis, R. G. Nuzzo, P. M. Ferreira, Y. G. Huang, A. Rockett, and J. A. Rogers, Nature Mater. **7**, 907 (2008).
[14] W. N. Peng, M. M. Roberts, E. P. Nordberg, F. S. Flack, P. E. Colavita, R. J. Hamers, D. E. Savage, M. G. Lagally, and M. A. Eriksson, Appl. Phys. Lett. **90**, 183107 (2007).
[15] A. Erbil, G. S. Cargill III, R. Frahm, and R. F. Boehme, Phys. Rev. B **37**, 2450 (1988).
[16] P. M. Mooney, G. M. Cohen, J. O. Chu, and C. E. Murray, Appl. Phys. Lett. **84**, 1093 (2004).
[17] M. L. Lee, D. A. Antoniadis, and E. A. Fitzgerald, Thin Solid Films **508**, 136 (2006).
[18] D. M. Paskiewicz, D. E. Savage, and M. G. Lagally (unpublished).
[19] A. C. Opotowsky, S. A. Scott, C. S. Ritz, D. E. Savage, G. K. Celler, and M. G. Lagally, New J. Phys. **9**, 270 (2007).
[20] E. M. Rehder, C. K. Inoki, T. S. Kuan, and T. F. Kuech, J. Appl. Phys. **94**, 7892 (2003).
[21] C. Euaruksakul, B. Yang, M. R. Kelly, D. E. Savage, and M. G. Lagally (unpublished).
[22] E. A. Fitzgerald, Y. H. Xie, D. Monroe, P. J. Silverman, J. M. Kuo, A. R. Kortan, F. A. Thiel, and B. E. Weir, J. Vac. Sci. Technol. B **10**, 1807 (1992).
[23] S. A. Scott, W. N. Peng, A. M. Kiefer, H. Q. Jiang, I. Knezevic, D. E. Savage, M. A. Eriksson, and M. G. Lagally, ACS Nano **3**, 1683 (2009).
[24] J. F. Morar, P. E. Batson, and J. Tersoff, Phys. Rev. B **47**, 4107 (1993).

[25] J. R. Chelikowsky and M. L. Cohen, Phys. Rev. B **10**, 5095 (1974).
[26] W. Eberhardt and F. J. Himpsel, Phys. Rev. B **21**, 5572 (1980).
[27] Website, http://www.ioffe.ru/SVA/NSM/Semicond/Si/basic.html
[28] G. P. Schwartz, M. S. Hybertsen, J. Bevk, R. G. Nuzzo, J. P. Mannaerts, and G. J. Gualtieri, Phys. Rev. B **39**, 1235 (1989).
[29] C. G. Van de Walle and R. M. Martin, Phys. Rev. B **34**, 5621 (1986).
[30] S. Richard, F. Aniel, G. Fishman, and N. Cavassilas, J. Appl. Phys. **94**, 1795 (2003).
[31] M. M. Rieger and P. Vogl, Phys. Rev. B **48**, 14276 (1993).
[32] D. Rideau, M. Feraille, L. Ciampolini, M. Minondo, C. Tavernier, H. Jaouen, and A. Ghetti, Phys. Rev. B **74**, 195208 (2006).
[33] M. V. Fischetti and S. E. Laux, J. Appl. Phys. **80**, 2234 (1996).
[34] C. Herring and E. Vogt, Phys. Rev. **101**, 944 (1956).
[35] J. M. Hinckley and J. Singh, Phys. Rev. B **42**, 3546 (1990).
[36] Y. H. Li, X. G. Gong, and S. H. Wei, Phys. Rev. B **73**, 245206 (2006).
[37] C. G. Van de Walle, Phys. Rev. B **39**, 1871 (1989).
[38] R. Schlaf, R. Hinogami, M. Fujitani, S. Yae, and Y. Nakato, J. Vac. Sci. Technol. A **17**, 164 (1999).
[39] J. B. Cui, J. Ristein, and L. Ley, Phys. Rev. Lett. **81**, 429 (1998).
[40] C. Tserbak and G. Theodorou, Phys. Rev. B **52**, 12232 (1995).
[41] C. G. Van de Walle and R. M. Martin, Phys. Rev. Lett. **62**, 2028 (1989).
[42] P. Ordejón, E. Artacho, and J. M. Soler, Phys. Rev. B **53**, R10441 (1996).
[43] L. Kleinman, Phys. Rev. B **24**, 7412 (1981).
[44] C. G. Van de Walle and R. M. Martin, Phys. Rev. B **35**, 8154 (1987).
[45] J. Junquera, M. Zimmer, P. Ordejón, and P. Ghosez, Phys. Rev. B **67**, 155327 (2003).
[46] Y. Sun, S. E. Thompson, and T. Nishida, J. Appl. Phys. **101**, 104503 (2007).